Microstructural evolution of pre-oxidized Cr-coated Zry-4 during annealing in argon

Junkai Liu[a, b, c, *], Ruizhi Meng[c], Martin Steinbrück[b], Mirco Große[b], Ulrike Stegmaier[b], Chongchong Tang[b], Jianqiao Yang[c, d], Di Yun[c, d]

[a] School of Advanced Materials and Nanotechnology, Xidian University, Xi'an 710126, China
[b] Institute for Applied Materials (IAM), Karlsruhe Institute of Technology (KIT), D-76021 Karlsruhe, Germany
[c] School of Nuclear Science and Technology, Xi'an Jiaotong University, Xi'an 710049, China
[d] Key Laboratory of Thermo-Fluid Science and Engineering of MOE, School of Energy and Power Engineering, Xi'an Jiaotong University, Xi'an 710049, PR China

ARTICLE INFO

Keywords:
Accident-tolerant fuel (ATF) cladding
Cr coating
Diffusion
Annealing
Pores

ABSTRACT

The annealing behavior of the pre-oxidized Cr-coated Zry-4 at 1200 °C in argon is systematically investigated. A Cr_2O_3 scale with a thickness of ~9 μm formed on the sample surface after pre-oxidation of the Cr-coated Zry-4 in steam at 1200 °C for 30 min. During annealing in inert atmosphere, the thickness of the Cr_2O_3 scale decreases with the increase of the annealing time because of the reaction between the Cr_2O_3 scale and the outward diffused Zr at the Cr_2O_3/Cr interface, the decomposition of Cr_2O_3, and the inward diffusion of O into the Zircaloy substrate along the ZrO_2 precipitates at the Cr grain boundaries. The Cr_2O_3 scale has completely transformed into Cr after annealing for one hour. Pores and Cr grains are observed inside the Cr_2O_3 scale after annealing due to the decomposition of Cr_2O_3. The ZrO_2 precipitates at Cr grain boundaries gradually grow outward during the annealing and finally reach the outer surface of the Cr coating. The results in this paper provide new insights into the thickness decrease mechanism and the decomposition behavior of the Cr_2O_3 scale.

1. Introduction

Since the Fukushima nuclear power plant accident in 2011, many research institutions, commercial companies, and universities have been engaged in the R&D of the accident tolerant fuels (ATFs), which were proposed to improve the safety of the current nuclear reactor fuels at the accident conditions [1–3]. Among many concepts of ATFs, Zircaloy substrate with surface Cr coating has been considered as one of the most promising ATF cladding candidate materials for industrial application due to its low research and development cost and time as well as the excellent performance of the Cr coating [4, 5]. Up to present, a large number of experiments have proven that surface Cr coating can effectively protect the Zircaloy substrate from oxidation and hence improve the performance of the current Zircaloy cladding materials under simulated loss of the coolant accident conditions [6–11].

However, during isothermal steam oxidation of the Cr-coated Zircaloy at high temperature, the coating failure and oxidation kinetics transition always occur before the complete consumption of Cr coating by steam oxidation [10–12]. According to the previous work by ourselves and other researchers [9–14], this type of coating failure should be attributed to the collective effects of the thickness decrease of the Cr_2O_3 scale, the outward diffusion of Zr, and the formation of ZrO_2 precipitates at the grain boundaries of unoxidized Cr coating. As regards the thickness decrease of the Cr_2O_3 scale, the most acceptable mechanism was proposed by Han [10] and ourselves [12] that the reaction between the Cr_2O_3 scale and the Zircaloy substrate (or the outward diffused Zr at Cr grain boundaries) reduces Cr_2O_3 into Cr. However, further evidence is needed to prove that this reaction is the most dominant factor for the reduction of the Cr_2O_3 scale.

Moreover, the in-depth microstructural evolution mechanism of the Cr_2O_3 scale is still unclear up to now. In our previous work about the isothermal steam oxidation of the Cr-coated Zry-4 samples [12], a lot of pores were observed inside the Cr_2O_3 scale during the thickness decrease of the Cr_2O_3 scale. A mechanism was proposed that the decomposition of Cr_2O_3 leads to the formation of pores based on the observation of amorphous Cr_2O_3 close to pores. The loss of O in Cr_2O_3 produces oxygen vacancies, which can trigger the order-disorder transformation of the oxide [15, 16]. The complete decomposition of Cr_2O_3 produces pores, while the

* Corresponding author.
E-mail address: liujunkai@xidian.edu.cn (J. Liu).

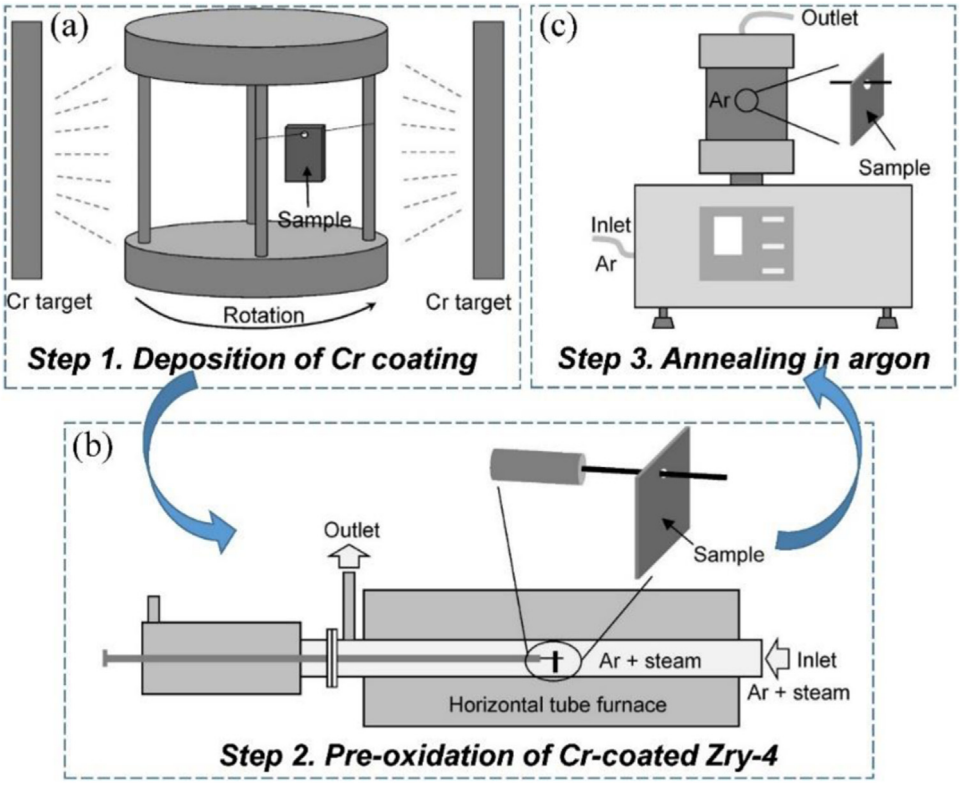

Fig. 1. Schematic of the whole experimental process.

incomplete decomposition results in the formation of amorphous Cr_2O_3. However, more direct evidence is needed to prove this hypothesis that the decomposition of Cr_2O_3 occurs inside the Cr_2O_3 scale at high temperature.

In order to further investigate the microstructural evolution mechanism of the Cr_2O_3 scale and to provide more evidence for the thickness decrease mechanism and the decomposition of the Cr_2O_3 scale at high temperature, annealing tests of pre-oxidized Cr-coated Zircaloy samples in argon were designed and conducted in this paper. During annealing in argon, no Cr_2O_3 can be produced by oxidation. Therefore, the microstructure and thickness of the Cr_2O_3 scale can only be affected by the interdiffusion between coating and substrate. The effect of the reaction between the Cr_2O_3 scale and the outward diffused Zr on the microstructure and thickness evolution behavior of the Cr_2O_3 scale can be clearly investigated.

In this paper, Cr-coated Zry-4 samples were first oxidized at 1200 °C in steam atmosphere for 30 min to form a thick Cr_2O_3 scale on the surface of the Cr coating, and then the pre-oxidized samples were annealed in argon atmosphere for different times. Eventually, the microstructures of the samples were studied, and the mechanisms were discussed.

2. Experimental

Fig. 1 shows the whole experimental process in this paper, which includes deposition of Cr coating on Zry-4, pre-oxidation of Cr-coated Zry-4 in the steam atmosphere, and annealing of the pre-oxidized Zry-4 in argon.

1) Step 1. Deposition of Cr coating

Cr coating with thickness ~17 μm was deposited on all six outer surfaces of the Zry-4 plates (15 mm×10 mm×0.65 mm) by magnetron sputtering. The specific coating deposition process has been introduced in our previous paper [12]. It is worth mentioning that the use of Zry-4 plates cannot fully represent the real Zry-4 cladding tube inside the reactor. Because the specific and grain morphologies are different between plates and tubes. Besides, there are internal stress inside the tubes.

2) Step 2. Pre-oxidation of the Cr-coated Zry-4

All Cr-coated Zry-4 plates were oxidized in a steam atmosphere (H_2O 20 g/h + Ar 20 L/h) at 1200 °C for 30 min by using a horizontal tube furnace (Fig. 1(b)). This furnace [17, 18] and the process of the oxidation tests [12, 19] were described in detail in our previous papers. The reason for choosing 30 min as the pre-oxidation time is that the oxidation kinetics transition of the Cr-coated Zry-4 samples in steam occurs at 30 min according to our previous isothermal steam oxidation tests at 1200 °C [12]. Moreover, the thickness of the Cr_2O_3 scale is at the largest value after oxidation for 30 min during the whole oxidation process, and then it will decrease with the increase of the oxidation time. It is worth mentioning that the transition time 30 min was just obtained by ourselves by using specific Cr-coated Zry-4 samples and specific oxidation condition. The transition time should vary depending on the samples and the test conditions.

3) Step 3. Annealing in argon

Subsequently, all pre-oxidized Cr-coated Zry-4 plates were annealed in an argon atmosphere (flow rate 50 mL/min) using a simultaneous thermal analysis (STA, NETZSCH STA449F3). The reason for choosing the STA to conduct the annealing tests is that this device can provide an oxygen-free environment (the oxygen concentration is less than 10^{-5} ppm at 1200 °C) to prevent further oxidation of the samples during annealing tests. Besides, a pure zirconium block was placed inside the STA to absorb residual oxygen. The actual temperature control curves of different samples are shown in Fig. 2. The heating and cooling rates of STA were controlled as 20 K/min and 100 K/min, respectively. When the sam-

Table 1
Mass changes of pre-oxidized samples during annealing in argon.

Sample	#A	#B	#C	#D	#E	#F
Mass changes (%)	−0.027	0.075	0.007	−0.040	−0.013	−0.005

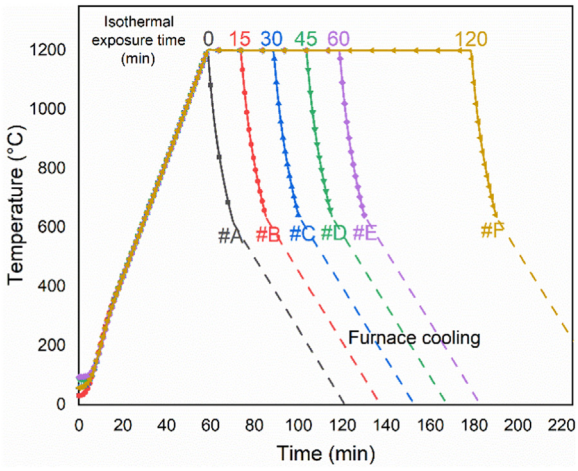

Fig. 2. Schematic temperature profiles of annealing tests.

ple temperature reached 1200 °C, the isothermal exposure stage started. The isothermal exposure times of #A, #B, #C, #D, #E, and #F samples at 1200 °C were controlled as 0 min, 15 min, 30 min, 45 min, 60 min, and 120 min, respectively. Thus, the #A sample with 0 min annealing time was only heated and then immediately cooled down.

Post-test examination

After the annealing tests, X-ray diffraction (XRD, Bruker D8 Focus) with a Cu Kα radiation source (λ = 1.54 Å) was used to study the surface phases of the Cr-coated samples. The 2θ range was 20–100°, and the scanning step was 0.02° The maximum penetration depths (when 2θ is 100°) of X-ray in Cr_2O_3 and Cr were calculated as ~8.587 μm and ~4.346 μm, respectively. The surface and cross-sectional microstructures of the pre-oxidized Cr-coated Zry-4 samples before and after the annealing tests were characterized by scanning electron microscopy (SEM, PhilipsXL30S and GeminiSEM 500) equipped with energy dispersive X-ray spectroscopy (EDS). The EDS measurement depths in Zr, Cr, and O were calculated as ~1.13 μm, ~1.00 μm, and ~4.18 μm, respectively. The specimens used for cross-sectional microstructural characterization were prepared by embedding in epoxy resin, grinding, polishing, ultrasonically cleaning, and drying.

3. Results

3.1. The microstructures of the as-deposited cr coating

Fig. 3 shows the surface and cross-sectional microstructures of the as-deposited Cr coating on the Zry-4 substrate. The average thickness of the as-deposited Cr coating is ~17.4 μm (Fig. 3(a)). The average grain size of the Cr coating is ~2 μm (Fig. 3(b)). The microstructure was also studied and reported in detail in our previous work [19].

3.2. The mass changes during annealing

Table 1 shows the mass changes data of pre-oxidized samples during annealing in argon. The mass changes of all samples are less than 0.08%, which should mainly be attributed to the measurement error. Moreover, there is no regularity between mass changes and annealing time. That indicates no volatilization or oxidation of samples occur during annealing in argon.

3.3. The surface phases

Fig. 4 shows the XRD patterns of the pre-oxidized Cr-coated Zry-4 samples before and after annealing in argon. In the pre-oxidized sample before annealing, only diffraction peaks of Cr_2O_3 are visible. This indicates that a thick Cr_2O_3 scale has formed on the outer surface of the coating after pre-oxidation. After annealing, peak (110) and peak (200) of Cr appear in all samples. Moreover, the intensity of these two peaks increases with the increase of the annealing time. After annealing for 60 min, the peaks of Cr_2O_3 entirely disappear, and only the peaks of Cr remain. That indicates all the Cr_2O_3 scale has transformed into Cr after annealing. It is worth mentioning that small peaks of the m-ZrO_2 phase were observed in almost all the samples, but only the high angle crystal plane (−132) of m-ZrO_2 is clear in the #F sample after annealing for 120 min. A peak of the t-ZrO_2 phase can be observed in very few samples, such as the #C sample. The appearance of the ZrO_2 peaks shows the formation of ZrO_2 close to the outer surface of the coating (the distance between ZrO_2 and the outer surface is less than the penetration depth 8.587 μm of X-ray in Cr_2O_3).

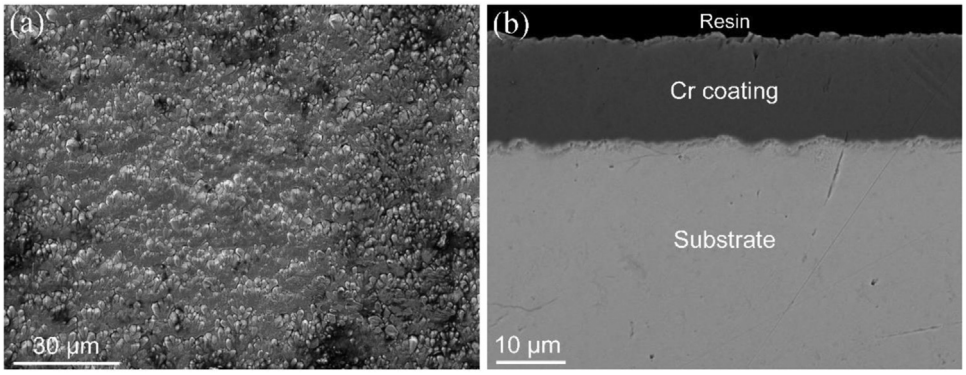

Fig. 3. (a) The surface and (b) cross-sectional SEM images of the as-deposited Cr-coating.

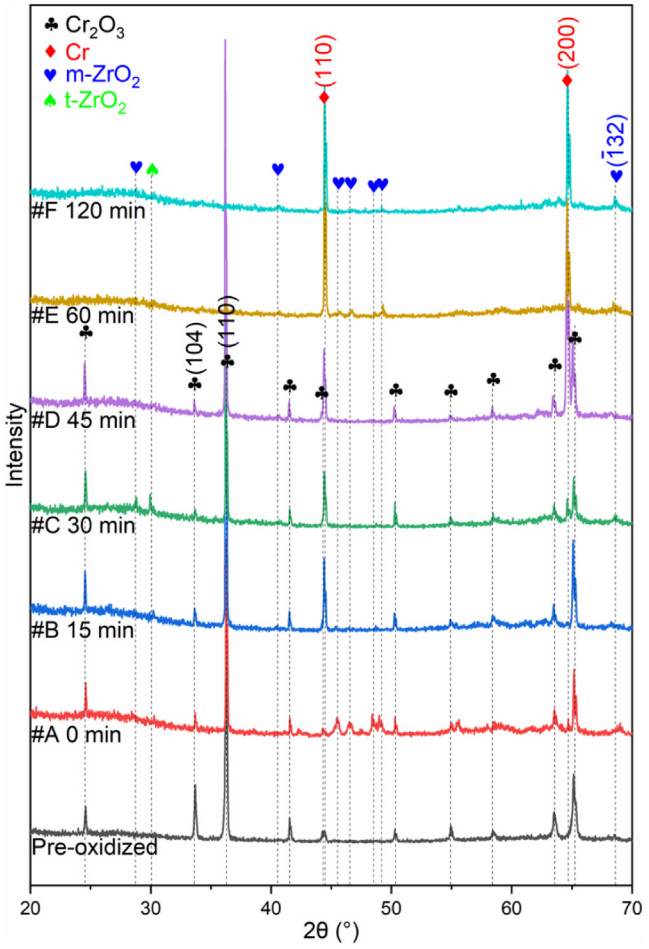

Fig. 4. XRD patterns of the pre-oxidized Cr-coated Zry-4 samples before and after annealing in argon.

Table 2
Semiquantitative elemental compositions on the surface of the #D sample in Fig. 5(e).

At.%	P1	P2	P3	P4
Cr	84	78	63	63
O	11	17	36	35
Fe	2	2	0	0
Zr	3	3	1	2

3.4. The surface microstructures

Fig. 5 displays the surface SEM micrographs of the pre-oxidized samples before and after isothermal annealing for 0–45 min. For isothermal annealing time (t) shorter than 30 min (Fig. 5(a), (b), and (c)), only Cr_2O_3 grains are observed on the surface of samples. However, after annealing for 30 min (Fig. 5(d)) and 45 min (Fig. 5(e)), there are larger particles distributed on the surface of the Cr_2O_3 scale. The semiquantitative elemental contents inside these particles are investigated by EDS maps in Fig. 5(f) (inside the white circle) and the EDS point analyses in Table 2. The contents of Cr in these particles are much higher than that in the oxide, while the compositions of O show the opposite trend that minimal O remains in these particles. The appearance of O should be due to the large EDS measurement depth of O (~4.18 μm) and Cr (~1 μm) and the small particle size (<1 μm). Therefore, these particles can be identified as Cr grains with a high probability for the following reasons: 1) no other Cr-rich phases were detected by XRD in Fig. 4 besides Cr and Cr_2O_3; 2) the contents of Fe and Zr in these particles are very small so there won't be another type of intermetallic; 3) only the Cr_2O_3 phase is stable at such a temperature so there won't be another type of oxide of Cr. The appearance of Cr grains on the surface of the Cr_2O_3 scale was rarely reported by other researchers in the field of Cr coating and Cr_2O_3 oxide. Besides, a minimal amount of Fe segregates inside these particles. This part of Fe should have diffused from the Zry-4 substrate. The enrichment of Fe is attributed to the high affinity between Fe and Cr, which was also observed in our previous work in the very late stage during the steam oxidation of Cr-coated Zry-4 [19].

Fig. 6 shows the surface SEM micrographs of the pre-oxidized samples after isothermal annealing for 60 min and 120 min. According to the XRD results in Fig. 4, the Cr_2O_3 scale has completely transformed into a Cr coating on the surface of these two samples. As can be seen in Fig. 6(a), after annealing for 60 min, many pores are distributed on the surface of the Cr coating. In the SEM image with a higher magnification (Fig. 6(b)), small white precipitates scatter on the surface of the Cr coating. These precipitates are located not only at the grain boundaries of Cr but also inside the Cr grains. These white precipitates can be identified as ZrO_2 based on the XRD results in Fig. 4 and the EDS maps in Fig. 6(c). When t increases to 120 min (Fig. 6(d)), the concentration of pores distinctly decreases on the surface of Cr coating, and the Cr grains grow up to some extent due to the sintering effect. Most white ZrO_2 particles have a larger size and are distributed at the grain boundaries of Cr (Fig. 6(e)). The EDS maps in Fig. 6(f) show further proof of the appearance of ZrO_2. The formation of ZrO_2 grains at the Cr grain boundaries has been regularly observed during the oxidation of the Cr-coated Zircaloy at high temperatures [10, 11, 13].

The average size of Cr_2O_3 and Cr grains was measured on the surface of all seven samples, and the results are summarized in Fig. 7. The error bar in Fig. 7 indicates the standard deviation of the grain size. Table 3 summarizes the total number of grains used for the measurement of grain size in Fig. 7. Obviously, when the surface Cr_2O_3 grains have not completely transformed into Cr ($t \leq 45$ min), the size of Cr_2O_3 grains increases with the increase of t. The grain size and the quantity of these Cr grains protruding on the surface increase when t increases from 30 min to 45 min. The grains of Cr coating also grow to some extent when t increases from 60 min to 120 min. The grain size of Cr coating ($t \geq 60$ min) is much larger than that of the Cr particles on the surface of the Cr_2O_3 scale (#C and #D sample).

3.5. The cross-sectional microstructures

Fig. 8 shows the cross-sectional microstructures of the pre-oxidized samples before and after annealing in argon atmosphere. Before t reaches 60 min (Fig. 8(a)–(f)), there are typical triple-layer structures of the coating: outer Cr_2O_3 scale, middle unoxidized Cr with ZrO_2 grains distributed on its grain boundaries (Fig. 8(d)), and inner $ZrCr_2$, which have been comprehensively investigated in the work of ourselves and other researchers [11, 12]. It is worth mentioning that the ZrO_2 precipitates at the Cr grain boundaries in the pre-oxidized sample (Fig. 8(a)) have reached the Cr_2O_3/Cr interface [12]. Pores can be observed inside the Cr_2O_3 scale (Fig. 8(b), (c), and (d)) after annealing, and similar pores were also observed in our previous work during the isothermal oxidation of the Cr-coated Zry-4 [12]. Moreover, small white particles are distributed inside the Cr_2O_3 scale and on the outer surface of the Cr_2O_3 scale (Fig. 8(c)–(g)). The semiquantitative EDS point analysis results of the white particle at P5 and the Cr_2O_3 scale at P6 in Fig. 8(g) are listed in Table 4. According to the EDS maps in Fig. 8(d) (inside the yellow circle) and the elemental compositions in Table 4, the content of Cr in these white particles is much higher than that in the Cr_2O_3 scale, also minimal Fe is detected inside these particles, which is similar with the results at P1 and P2 in Fig. 5(e). There-

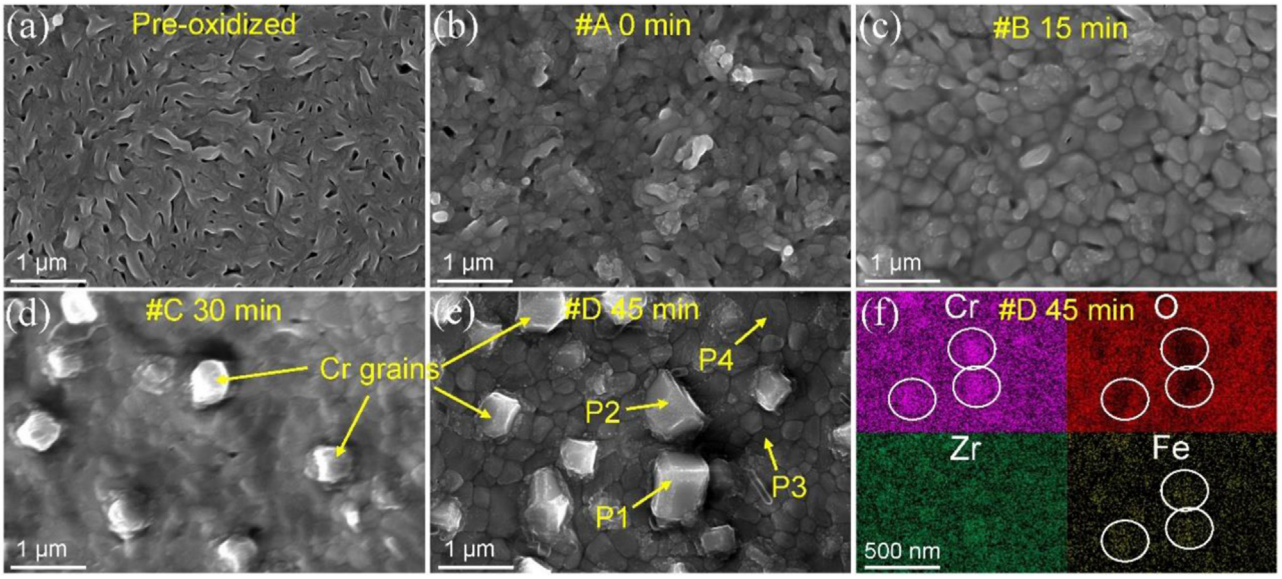

Fig. 5. Surface SEM images of the pre-oxidized Cr-coated Zry-4 before and after annealing in argon: (a) pre-oxidized; (b) #A sample; (c) #B sample; (d) #C sample; (e) #D sample; (f) EDS maps of (e).

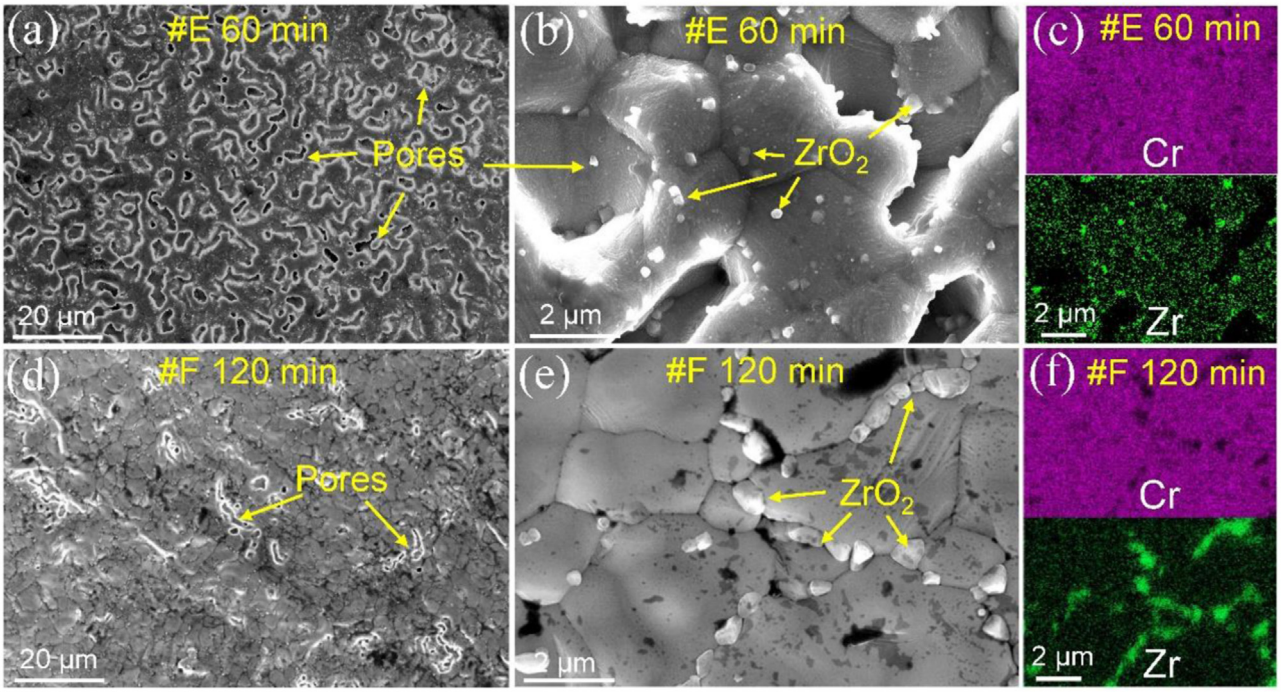

Fig. 6. Surface SEM images of the pre-oxidized Cr-coated Zry-4 after annealing in argon: (a) #E sample in low-magnification; (b) #E sample in high-magnification; (c) EDS maps of (b); (d) #F sample in low-magnification; (e) #F sample in high-magnification; (f) EDS maps of (e).

fore, these white particles should be Cr, and the particles on the surface of the Cr_2O_3 scale in Fig. 8(e)–(g) should be the Cr particles observed on the surface of the samples in Fig. 5(d) and (e).

At the local position of the #D sample after isothermal annealing for 45 min, as shown in Fig. 8(h) and (i), the Cr_2O_3 scale has entirely transformed into Cr. Hence the triple-layer coating transforms into a double-layer coating with outer Cr coating and inner $ZrCr_2$. According to the EDS maps in Fig. 8(i), a lot of ZrO_2 particles are distributed inside the Cr coating, and these ZrO_2 particles extend from the $ZrCr_2$ layer to the outer surface of the Cr coating. Inside the Zry-4 substrate (Fig. 8(h)), long dark grains saturate the bright Zry-4. These dark grains are Cr-Zr intermetallic compounds, which are produced during cooling stage because of the inward diffusion of Cr from Cr coating to the substrate and the solubility of Cr in Zr decreases during cooling [9, 12].

Fig. 9 shows the cross-sectional SEM micrographs of the pre-oxidized samples after isothermal annealing for 60 min and 120 min. The outer Cr_2O_3 scale has completely transformed into Cr, which is consistent with the surface SEM results in Fig. 6. Large pores are distributed inside the Cr coating close to the outer sur-

Table 3
The total number of grains used for the grain size measurement in Fig. 7.

Samples	Pre-oxi	#A	#B	#C	#D	#E	#F
Number of Cr grains	/	/	/	32	27	176	153
Number of Cr_2O_3 grains	223	279	186	194	163	/	/

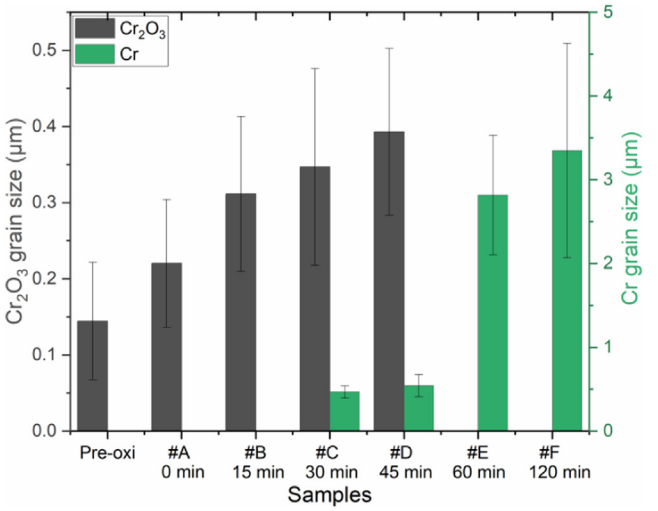

Fig. 7. Summary of the average grain size of Cr_2O_3 and Cr on the surface of each sample.

face. These pores should be the pores observed from the surface of the sample in Fig. 6(a) and (d). Based on the EDS maps in Fig. 9(c), the content of ZrO_2 particles inside the Cr coating is much smaller compared with the results in Fig. 8(i).

Table 4
Semiquantitative elemental compositions of P5 and P6 in Fig. 8(g).

At.%	P5	P6
Cr	67	41
O	27	57
Fe	1	0
Zr	5	2

The average thicknesses of the whole coating and each sublayer of different samples after annealing in argon are summarized in Fig. 10. With the increase of *t*, the thickness of the outer Cr_2O_3 scale decreases, and the thickness of the middle unoxidized Cr layer increases. The thickness of the inner $ZrCr_2$ layer does not change too much. It takes only 60 min to completely transform the Cr_2O_3 scale into Cr by annealing under inert atmosphere. After isothermal annealing for 120 min, the thickness of the unoxidized Cr coating decreases slightly, which should be attributed to the inward diffusion of Cr from the Cr coating to the Zircaloy substrate. The thickness of the outer Cr_2O_3 scale after annealing is smaller

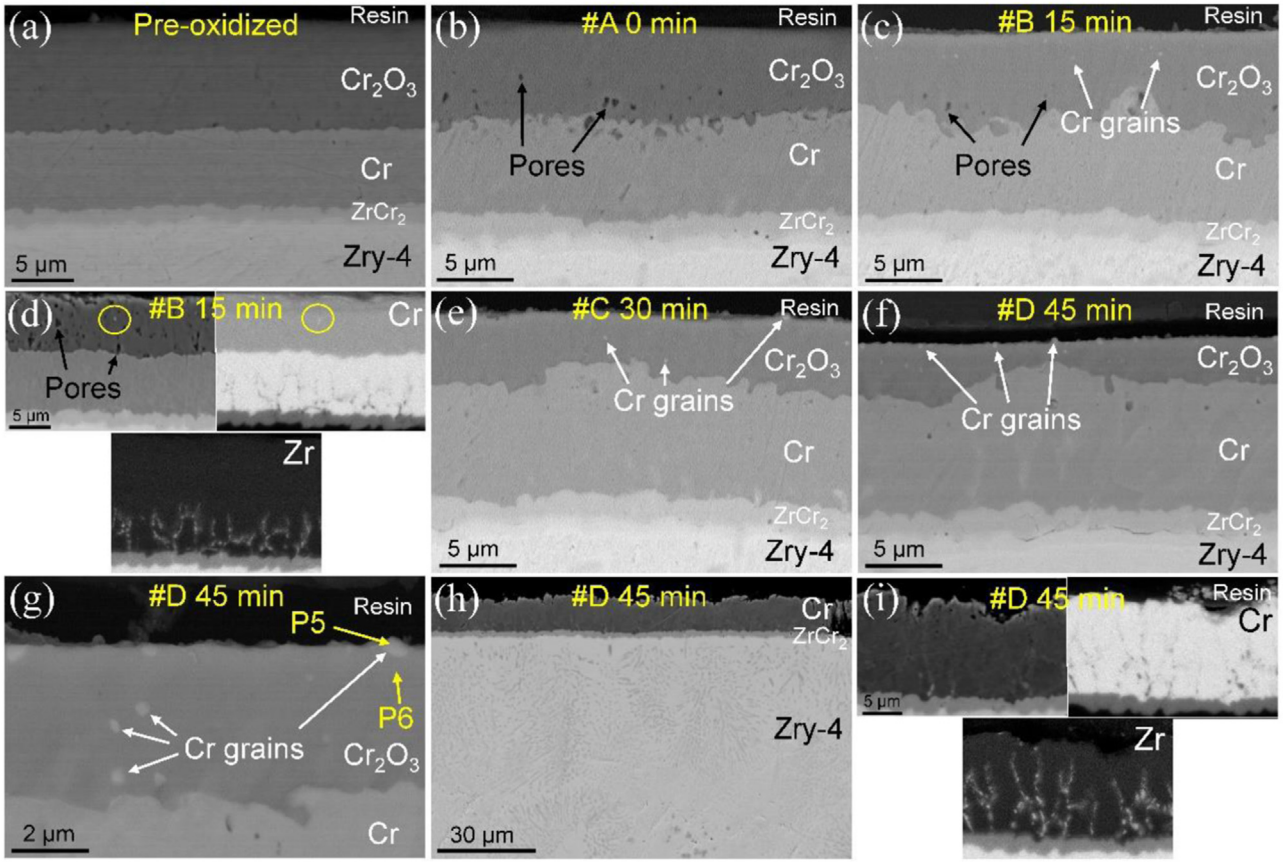

Fig. 8. Cross-sectional SEM images of the pre-oxidized Cr-coated Zry-4 before and after annealing in argon: (a) pre-oxidized; (b) #A sample; (c) #B sample; (d) EDS maps of #B sample; (e) #C sample; (f) #D sample; (g) #D sample in high-magnification; (h) the Zry-4 substrate of #D sample; (i) EDS maps at local region of #D sample.

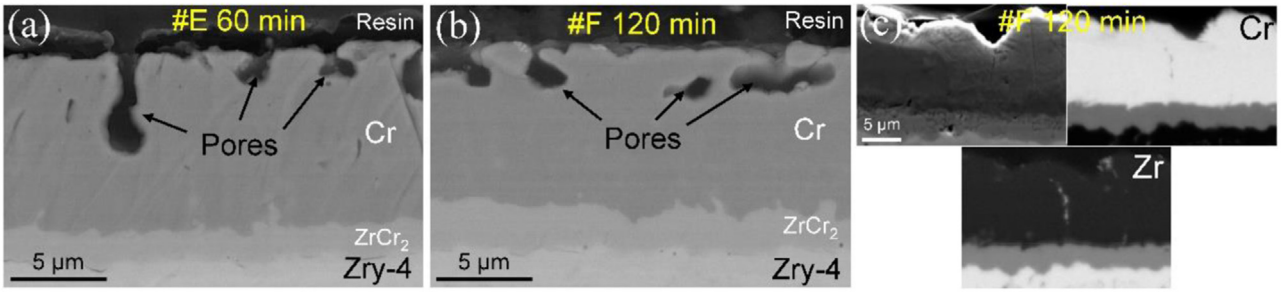

Fig. 9. Cross-sectional SEM images of the pre-oxidized Cr-coated Zry-4 after annealing in argon: (a) #E sample; (b) #F sample; (c) EDS maps of #F sample.

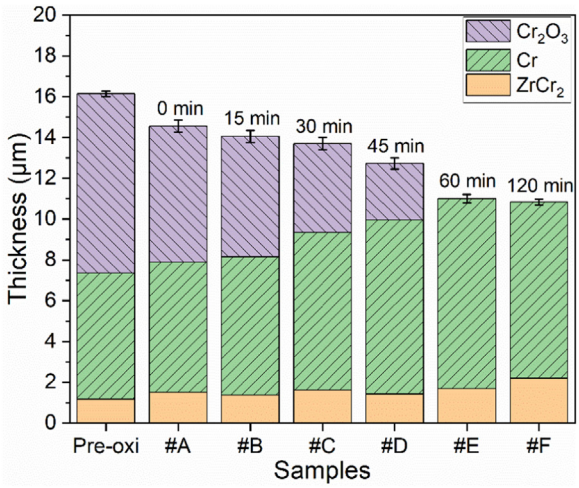

Fig. 10. Thickness evolution of the coating and each sublayer within the coating of different samples.

than the penetration depth of the X-ray in Cr_2O_3 (8.587 μm), and this is the reason why the peaks of Cr and ZrO_2 appears in all the samples after annealing.

4. Discussion

4.1. The thickness decrease mechanism of the Cr_2O_3 scale

During the steam oxidation of Cr-coated Zry-4, the thickness decrease of the outer Cr_2O_3 scale was observed and reported by ourselves and other researchers [9, 10, 12, 19] after the Cr_2O_3 scale grew to a certain thickness by steam oxidation. A mechanism was proposed that the reaction between the outward diffused Zr at the unoxidized Cr grain boundaries and the Cr_2O_3 scale at the Cr_2O_3/Cr interface is the main factor for the reduction of the Cr_2O_3 scale [12]. As shown in Eq. (1), this reaction consumes Cr_2O_3 but produces ZrO_2 at the Cr_2O_3/Cr interface. Considering the reaction products between Zr and the Cr_2O_3 scale, only the Cr and ZrO_2 phases were detected by XRD (Fig. 4). This result is consistent with Eq. (1). The formation of metastable (Cr, Zr)$_2O_3$ phase was reported by other researchers in the Cr-Zr-O system [20–22]. But this phase is unstable and will decompose into Cr_2O_3 and ZrO_2 phases at 1000 °C [20]. Moreover, according to the ZrO_2-Cr_2O_3 phase diagram, no intermediate phase can form between the ZrO_2 and the Cr_2O_3 phases at 1200 °C [23]. Therefore, only ZrO_2 and Cr phases can form during the annealing of the pre-oxidized Cr-coated Zry-4 samples.

The schematic of the microstructural evolution of the coating in inert atmosphere (preventing further oxidation) is shown in Fig. 11. The times for the various degradation steps in Fig. 11 may vary for different coatings, but the general mechanism should be valid for all Cr coatings. During the annealing tests of the pre-oxidized Cr-coated Zry-4, the Cr_2O_3 scale with a thickness of ~9 μm has totally disappeared within only an hour, which is a very short time. Moreover, by comparing the position of ZrO_2 particles at the Cr grain boundaries at t = 15 min (Fig. 8(d)) and t = 45 min (Fig. 8(i)), a correlation can be seen between the ZrO_2 precipitates, which grow gradually towards the outer surface of the coating, and the decrease in the thickness of the Cr_2O_3 layer. The front of the ZrO_2 particles is always located at the Cr_2O_3/Cr interface (Fig. 11(a)–(c)). When Cr_2O_3 has entirely transformed into Cr, these ZrO_2 precipitates finally reach the outer surface of the Cr coating (Fig. 11(c) and (d)). These results obtained from the annealing tests of the pre-oxidized Cr-coated Zry-4 provide direct evidence that it is mainly the reaction of Eq. (1) at the Cr_2O_3/Cr interface leads to the thickness decrease of the Cr_2O_3 scale. In other words, the interdiffusion between the surface coating and the Zircaloy substrate, especially the outward diffusion of Zr at unoxidized Cr grain boundaries, is the primary reason for the thickness decrease of the Cr_2O_3 scale.

$$3Zr + 2Cr_2O_3 \rightarrow 3ZrO_2 + 4Cr \quad (1)$$

Moreover, the decomposition of Cr_2O_3 scale at the Cr_2O_3/Cr interface was also proposed in our previous work according to the formation of pores and amorphous phase at the Cr_2O_3/Cr interface [12]. Because the amorphization of Cr_2O_3 just occurs at very small region of Cr_2O_3 (edge region of the pores), the XRD peaks broadening of Cr_2O_3 cannot be observed in Fig. 4. O atoms produced by the decomposition of Cr_2O_3 can also be absorbed by Zry-4 substrate through the inward diffusion of O along the ZrO_2 precipitates at Cr grain boundaries to the Zircaloy substrate since ZrO_2 is a very good conductor of O (Fig. 10(b)). Also, O atoms are much smaller than Zr atoms, which diffuse much faster. The high solid solubility of oxygen in Zry-4 determines that the Zry-4 substrate can serve as excellent oxygen absorber. The inward diffusion of O should be another important reason for the reduction of the Cr_2O_3 scale. This is the reason why there is no thick ZrO_2 layer forms when the Cr_2O_3 scale has completely transformed to Cr. However, further work is necessary to better assess that if there are any reasons for the disappearance of the oxygen produced by the decomposition of Cr_2O_3.

4.2. The formation mechanism of pores and Cr grains inside the Cr_2O_3 scale

Pores inside the Cr_2O_3 scale were also observed in our previous work during the isothermal oxidation of Cr-coated Zry-4 in steam atmosphere [12]. A mechanism was proposed that the decomposition of Cr_2O_3 grain occurs inside the Cr_2O_3 scale. The complete decomposition of Cr_2O_3 produces O and Cr. O can be absorbed by inner Zr at the Cr grain boundaries. Cr can diffuse outward to the steam/Cr_2O_3 interface and form a new Cr_2O_3 scale at the outer surface of the coating. Therefore, the decomposition of Cr_2O_3 results in the formation of pores. This is why the Cr_2O_3 scale cannot en-

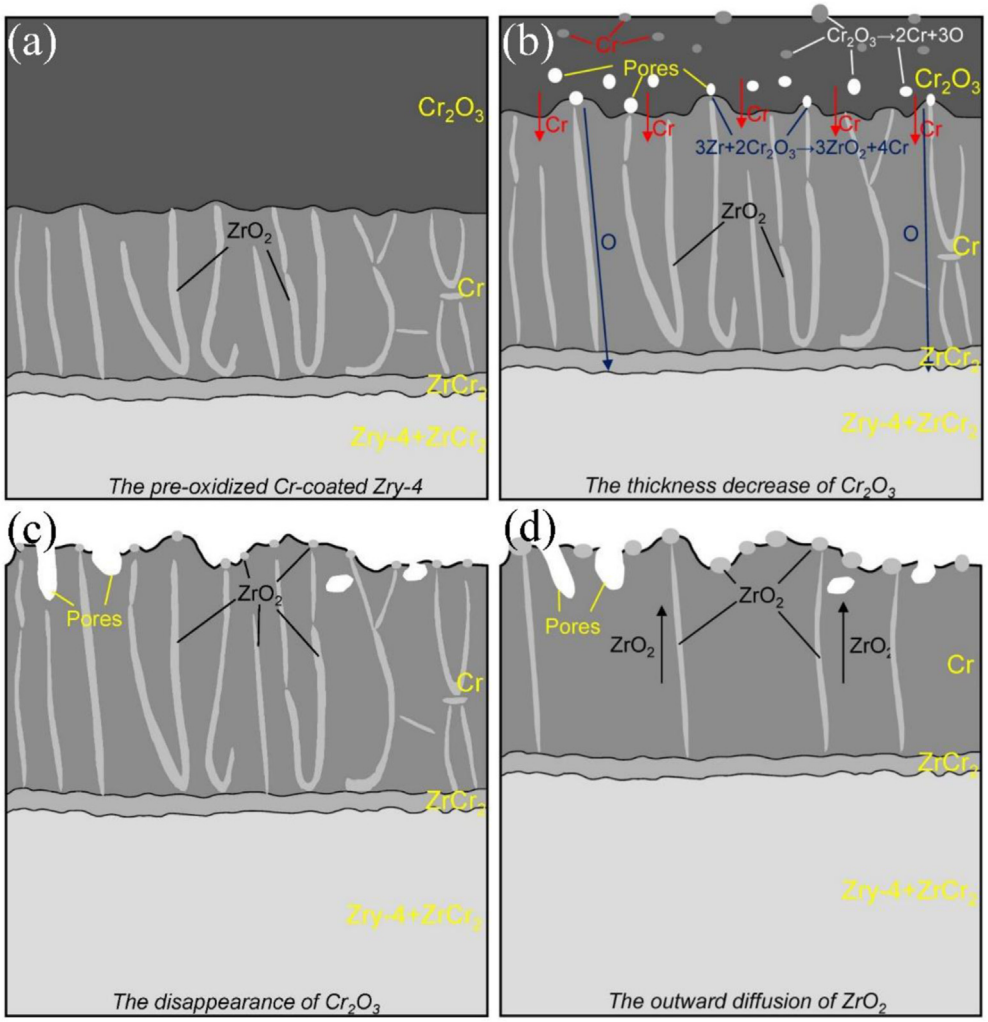

Fig. 11. Schematic of the microstructural evolution of the pre-oxidized Cr-coated Zry-4 during the isothermal annealing in argon: (a) the pre-oxidized Cr-coated Zry-4; (b) the thickness decrease of the Cr_2O_3 scale; (c) the disappearance of the Cr_2O_3 scale; (d) the outward diffusion of Zr^{4+} and O^{2-} ions in ZrO_2 at the Cr grain boundaries.

tirely disappear during steam oxidation. However, in the current annealing tests without a steam atmosphere, a significant phenomenon was observed that Cr grains form inside the Cr_2O_3 scale (Fig. 8(e)–(g)) and even on the outer surface of the Cr_2O_3 scale (Fig. 5(d) and (e)). The appearance of Cr grains inside the Cr_2O_3 scale after annealing provide direct evidence for the decomposition of Cr_2O_3 at high temperatures. The decomposition behavior of Cr_2O_3 was rarely reported by other researchers in the field of Cr_2O_3 at high temperature. Wang et al. [24] observed the sublimation behavior of Cr_2O_3 at high temperatures in a vacuum. Besides, Beruto et al. [25] and Peres [26] investigated the volatility of Cr_2O_3 in vapor at high temperatures. All these works indicate that Cr_2O_3 can decompose into gaseous Cr or CrO and gaseous O_2, which are pretty different from the phenomenon observed in the current work. Therefore, the decomposition of Cr_2O_3 inside the Cr_2O_3 scale is a particular case in this paper, which should be related to the outward diffused Zr at the Cr grain boundaries and the reaction at the Cr_2O_3/Cr interface.

The formation mechanism of pores inside the Cr_2O_3 should be attributed to the decomposition of Cr_2O_3 and the inward diffusion of the produced Cr into the unoxidized Cr layer and the inward diffusion of O to the Zircaloy substrate (Fig. 11(b)). On the one hand, there is no oxidizing atmosphere surrounding the outer surface of the coating during annealing in argon, and hence there is no driving force for the outward diffusion of Cr to the outer surface of the coating. On the other hand, pores inside the Cr_2O_3 scale are distributed close to the Cr_2O_3/Cr interface (Fig. 8(c)–(d)), which is consistent with the fact that Cr close to the Cr_2O_3/Cr interface can easier diffuse into the unoxidized Cr layer. This type of pores inside the Cr_2O_3 scale was also observed during the oxidation of Cr metal under a water vapor atmosphere [27]. In that case, the formation mechanism of these pores is due to the vacancy condensation at the Cr_2O_3/Cr interface rather than the direct decomposition of Cr_2O_3. With the further oxidation of Cr beneath the pores, these pores at Cr_2O_3/Cr interface can gradually move into the center of the Cr_2O_3 scale. However, no new Cr_2O_3 can form during the annealing of the Cr-coated Zry-4 under argon in the current experiment.

4.3. The formation mechanism of pores on the surface of the Cr coating

The formation of pores on the surface of the Cr coating after annealing for 60 min and 120 min should be related to the volume shrinkage of Eq.1 during the transformation of Cr_2O_3 to Cr. When all the materials are in a stress-free state, there is a ~8.35% volume shrinkage of Eq. (1) calculated by using the densities Zr: 6.49 g/cm^3, Cr_2O_3: 5.21 g/cm^3, ZrO_2: 5.85 g/cm^3, Cr: 7.19 g/cm^3. Moreover, if the oxygen produced by the decomposition of Cr_2O_3 was absorbed by the Zry-4 substrate but not form ZrO_2 particles

inside the Cr coating, the volume shrinkage should be much larger than ~8.35%. After annealing for 60 min, the formation of pores on the surface of the Cr coating should be because of the volume shrinkage. With the annealing time increasing to 120 min, the thermal growth of Cr grains (Fig. 7) can fill up partially pores. Therefore, the concentration of pores decreases significantly. After the Cr_2O_3 scale has completely transformed into Cr, the Zr^{4+} and O^{2-} ions in ZrO_2 precipitates at the Cr grain boundaries can gradually diffuse towards the outer surface of the Cr coating with the growth of the Cr grains. Thereafter, ZrO_2 particles can be observed on the surface of the Cr coating (Fig. 11(c) and (d)), and only partial ZrO_2 particles remain inside the Cr coating (Fig. 11(d)).

5. Conclusions

Cr-coated Zry-4 samples were firstly oxidized in a steam atmosphere to form a Cr_2O_3 scale with a thickness of ~9 μm. Then the pre-oxidized samples with triple-layer Cr_2O_3/Cr/$ZrCr_2$ coating were annealed at 1200 °C in argon. The isothermal annealing behavior of the pre-oxidized samples was systematically investigated in the current paper. The microstructural evolution mechanism of the coating was discussed. The results in this paper provide ample evidence and new insights into the degradation mechanism of Cr-coated Zry-4. Several crucial conclusions are drawn from the obtained results:

1) The thickness of the Cr_2O_3 scale decreases with the increase of annealing time; the Cr_2O_3 scale has completely disappeared after annealing for only one hour.

2) The thickness decrease of the Cr_2O_3 scale and the outward diffusion of Zr at Cr grain boundaries during annealing in argon provide direct evidence that the reaction between Cr_2O_3 and Zr at the Cr_2O_3/Cr interface, the decomposition of Cr_2O_3, and the inward diffusion of O lead to the reduction of the Cr_2O_3 scale.

3) There are pores and Cr grains forming inside the Cr_2O_3 scale during the annealing tests, which provide direct evidence that the decomposition of Cr_2O_3 occurs inside the Cr_2O_3 scale at high temperature.

4) After the Cr_2O_3 scale has entirely transformed into Cr, pores form inside the Cr coating due to the volume shrinkage of the transformation from Cr_2O_3 to Cr.

5) ZrO_2 precipitates at Cr grain boundaries can gradually grow outward during the annealing tests and finally reach the outer surface of the Cr coating.

Declaration of Competing Interest

The authors declare that they have no known competing financial interests or personal relationships that could have appeared to influence the work reported in this paper.

CRediT authorship contribution statement

Junkai Liu: Conceptualization, Methodology, Investigation, Writing – original draft. **Ruizhi Meng:** Investigation, Methodology. **Martin Steinbrück:** Conceptualization, Project administration, Writing – review & editing. **Mirco Große:** Conceptualization, Writing – review & editing. **Ulrike Stegmaier:** Investigation, Writing – review & editing. **Chongchong Tang:** Investigation, Methodology, Writing – review & editing. **Jianqiao Yang:** Resources. **Di Yun:** Supervision.

Data availability

Data will be made available on request.

Data availability

The raw data required to reproduce these findings cannot be shared at this time as the data also forms part of an ongoing study. The processed data required to reproduce these findings cannot be shared at this time as the data also forms part of an ongoing study.

Acknowledgments

The work was conducted in the framework of the HGF program NUSAFE. The authors thank Petra Severloh for her support in the sample preparation.

References

[1] K.A. Terrani, Accident tolerant fuel cladding development: promise, status, and challenges, J. Nucl. Mater. 501 (2018) 13–30.
[2] S.J. Zinkle, K.A. Terrani, J.C. Gehin, L.J. Ott, L.L. Snead, Accident tolerant fuels for LWRs: a perspective, J. Nucl. Mater. 448 (1–3) (2014) 374–379.
[3] L.J. Ott, K.R. Robb, D. Wang, Preliminary assessment of accident-tolerant fuels on LWR performance during normal operation and under DB and BDB accident conditions, J. Nucl. Mater. 448 (1–3) (2014) 520–533.
[4] C. Tang, M. Stueber, H.J. Seifert, M. Steinbrueck, Protective coatings on zirconium-based alloys as accident-tolerant fuel (ATF) claddings, Corros. Rev. 35 (3) (2017) 141–165.
[5] J. Yang, M. Steinbrück, C. Tang, M. Große, J. Liu, J. Zhang, D. Yun, S. Wang, Review on chromium coated zirconium alloy accident tolerant fuel cladding, J. Alloys Compd. 895 (2022) 162450.
[6] J.-C. Brachet, I. Idarraga-Trujillo, M.Le Flem, M.Le Saux, V. Vandenberghe, S. Urvoy, E. Rouesne, T. Guilbert, C. Toffolon-Masclet, M. Tupin, Early studies on Cr–Coated Zircaloy-4 as enhanced accident tolerant nuclear fuel claddings for light water reactors, J. Nucl. Mater. 517 (2019) 268–285.
[7] H.-G. Kim, I.-H. Kim, Y.-I. Jung, D.-J. Park, J.-Y. Park, Y.-H. Koo, Adhesion property and high-temperature oxidation behavior of Cr-coated Zircaloy-4 cladding tube prepared by 3D laser coating, J. Nucl. Mater. 465 (2015) 531–539.
[8] F. Qi, Z. Liu, Q. Li, H. Yu, P. Chen, Y. Li, Y. Zhou, C. Ma, C. Tang, Y. Huang, Pellet-cladding mechanical interaction analysis of Cr-coated Zircaloy cladding, Nucl. Eng. Des. 367 (2020) 110792.
[9] X. Han, J. Xue, S. Peng, H. Zhang, An interesting oxidation phenomenon of Cr coatings on Zry-4 substrates in high temperature steam environment, Corros. Sci. 156 (2019) 117–124.
[10] X. Han, C. Chen, Y. Tan, W. Feng, S. Peng, H. Zhang, A systematic study of the oxidation behavior of Cr coatings on Zry4 substrates in high temperature steam environment, Corros. Sci. 174 (2020) 108826.
[11] J.-C. Brachet, E. Rouesne, J. Ribis, T. Guilbert, S. Urvoy, G. Nony, C. Toffolon–Masclet, M.Le Saux, N. Chaabane, H. Palancher, High temperature steam oxidation of chromium-coated zirconium-based alloys: kinetics and process, Corros. Sci. 167 (2020) 108537.
[12] J. Liu, M. Steinbrück, M. Große, U. Stegmaier, C. Tang, D. Yun, J. Yang, Y. Cui, H.J. Seifert, Systematic investigations on the coating degradation mechanism during the steam oxidation of Cr-coated Zry-4 at 1200°C, Corros. Sci. 202 (2022) 110310.
[13] J. Liu, Z. Cui, Z. Hao, D. Ma, J. Lu, Y. Cui, C. Li, W. Liu, S. Xie, P. Hu, Steam oxidation of Cr-coated Sn-containing Zircaloy solid rod at 1000°C, Corros. Sci. 190 (2021) 109682.
[14] M. Steinbrück, U. Stegmaier, M. Große, L. Czerniak, E. Lahoda, R. Daum, K. Yueh, High-temperature oxidation and quenching of chromium-coated zirconium alloy ATF cladding tubes with and w/o pre-damage, J. Nucl. Mater. 559 (2022) 153470.
[15] X. Lü, Q. Hu, W. Yang, L. Bai, H. Sheng, L. Wang, F. Huang, J. Wen, D.J. Miller, Y. Zhao, Pressure-induced amorphization in single-crystal Ta2O5 nanowires: a kinetic mechanism and improved electrical conductivity, J. Am. Chem. Soc. 135 (37) (2013) 13947–13953.
[16] N. Kawai, T. Atou, S. Ito, K. Yubuta, M. Kikuchi, K.G. Nakamura, K.-i. Kondo, Aligned nanocrystalline fragmentation of mullite under shock loading, Adv. Mater. 19 (17) (2007) 2375–2378.
[17] M. Steinbrück, Oxidation of boron carbide at high temperatures, J. Nucl. Mater. 336 (2–3) (2005) 185–193.
[18] J. Yang, U. Stegmaier, C. Tang, M. Steinbrück, M. Große, S. Wang, H.J. Seifert, High temperature Cr-Zr interaction of two types of Cr-coated Zr alloys in inert gas environment, J. Nucl. Mater. 547 (2021) 152806.
[19] J. Liu, C. Tang, M. Steinbrück, J. Yang, U. Stegmaier, M. Grosse, D. Yun, H.J. Seifert, Transient experiments on oxidation and degradation of Cr-coated Zircaloy in steam up to 1600°C, Corros. Sci. 192 (2021) 109805.
[20] M. Mohammadtaheri, Y. Li, J. Corona-Gomez, Q. Yang, An investigation on synthesis and characterization of superhard Cr-Zr-O coatings, Surf. Coat. Technol. 375 (2019) 694–700.
[21] L. Landälv, J. Lu, S. Spitz, H. Leiste, S. Ulrich, M. Johansson-Jõesaar, M. Ahlgren, E. Göthelid, B. Alling, L. Hultman, Structural evolution in reactive RF magnetron sputtered (Cr, Zr) 2O3 coatings during annealing, Acta Mater. 131 (2017) 543–552.

[22] D. Rafaja, C. Wüstefeld, G. Abrasonis, S. Braeunig, C. Baehtz, F. Hanzig, M. Dopita, M. Krause, S. Gemming, Thermally induced formation of metastable nanocomposites in amorphous Cr-Zr-O thin films deposited using reactive ion beam sputtering, Thin. Solid. Films 612 (2016) 430–436.
[23] D. Jerebtsov, G. Mikhailov, S. Sverdina, Phase diagram of the system: ZrO2–Cr2O3, Ceram. Int. 27 (3) (2001) 247–250.
[24] K.C. Wang, L.H. DREGER, V. Dadape, J.L. MARGRAVE, Sublimation of Cr2O3 at high temperatures, J. Am. Ceram. Soc. 43 (10) (1960) 509–510.
[25] D. Beruto, L. Barco, G. Belleri, On the stability of refractory materials under industrial vacuum conditions:: Al2O3, BeO, CaO, Cr2O3, MgO, SiO2, TiO2 systems, Ceramurgia Int. 1 (2) (1975) 87–93.
[26] V. Peres, L. Favergeon, M. Andrieu, J.C. Palussière, J. Balland, C. Delafoy, M. Pijolat, High temperature chromium volatilization from Cr2O3 powder and Cr2O3-doped UO2 pellets in reducing atmospheres, J. Nucl. Mater. 423 (1) (2012) 93–101.
[27] M. Michalik, M. Hänsel, J. Zurek, L. Singheiser, W. Quadakkers, Effect of water vapour on growth and adherence of chromia scales formed on Cr in high and low pO2-environments at 1000 and 1050 C, Mater. High Temp. 22 (3–4) (2005) 213–221.